ASTRONOMY
AND
ASTROPHYSICS

H₂ and its relation to CO in the LMC and other magellanic irregular galaxies

F.P. Israel

Sterrewacht Leiden, P.O. Box 9513, 2300 RA Leiden, The Netherlands

Abstract. H₂ column densities towards CO clouds in the LMC and SMC are estimated from their far-infrared surface brightness and HI column density. The newly derived H₂ column densities imply $N(H_2)/I(CO)$ conversion factors (in units of 10^{21} mol cm^{-2} (Kkms^{-1})$^{-1}$) $X_{LMC} = 1.3\pm0.2$ and $X_{SMC} = 12\pm2$. LMC and SMC contain total (warm) H₂ masses of $1.0\pm0.3 \times 10^8 \, M_\odot$ and $0.75\pm0.25 \times 10^8 \, M_\odot$ respectively. Local H₂/HI mass ratios similar to those in LMC and SMC are found in the magellanic irregulars NGC 55, 1569, 4214, 4449 and 6822 and in the extragalactic HII region complexes NGC 604, 595 and 5461 in M 33 and M 101 respectively. In these HII regions and in NGC 4449, we find $X = 1$–2; in NGC 55, 4214 and 6822 $X = 3$–6 again in units of 10^{21} mol cm^{-2} (Kkms^{-1})$^{-1}$. The post-starburst galaxy NGC 1569 has a very high value similar to that of the SMC.

The CO–H₂ conversion factor X is found to depend on both the ambient radiation field intensity per nucleon σ_{FIR}/N_H and metallicity [O]/[H]: $\log X \propto 0.9\pm0.1 \log\frac{\sigma_{FIR}}{N_H}$ - $3.5\pm0.2 \log\frac{[O]}{[H]}$. Neglecting dependency on radiation field, a reasonable approximation is also provided by $\log X \propto$ -2.7$\pm$0.3 $\log\frac{[O]}{[H]}$. Milky Way values are consistent with these relations. This result is interpreted as the consequence of selective photodissociation of CO subjected to high radiation field energy densities and poor (self)shielding in low-metallicity environments, and especially the preferential destruction of diffuse CO in 'interclump' gas.

Although locally H₂ may be the dominant ISM-component, the average global H₂/HI mass ratio is 0.2 ± 0.04 and the average H₂ gas mass fraction is 0.12 ± 0.02. Magellanic irregulars have warm molecular gas fractions very similar to those of our Galaxy, whereas other global properties (mass, luminosity, metallicity, CO luminosity) are very different.

Key words: Galaxies: individual: LMC; SMC – Galaxies: ISM; irregular; Magellanic Clouds – Infrared: ISM: continuum – ISM: molecules

1. Introduction

1.1. H₂ content of galaxies

The existence of molecular hydrogen (H₂) in interstellar space was suggested as early as 60 years ago by Eddington (1937) and Strömgren (1939). Thirty years later, Gould & Salpeter (1963) and Hollenbach et al. (1971) predicted that it could be a large fraction of all hydrogen. However, H₂ is difficult to observe directly, because it is a symmetrical molecule lacking a dipole moment. Nevertheless, it has been observed in absorption at UV wavelengths and in emission at infrared wavelengths. Because the emission arises mostly in warm or hot molecular gas, it has been virtually impossible to deduce total amounts of H₂ which is expected to be present mostly at low temperatures.

As H₂ is an abundant and important constituent of the interstellar medium in galaxies, there has been great interest in determining its presence and properties. Because it is commonly assumed that star formation requires interstellar clouds to pass through a cool, high-density phase in which most of the hydrogen is in molecular form, studies of star formation in external galaxies also seek to determine H₂ amounts in such galaxies.

Emission from the tracer CO molecule has been and still is widely used to determine the distribution and amount of molecular hydrogen in our own Milky Way and other galaxies. Although the usually optically thick ^{12}CO emission does not provide direct information on column densities, empirical relations between CO luminosities and virial masses of molecular clouds in the Galaxy suggest that circumstances nevertheless allow its use in an indirect manner. The underlying thought is that CO is distributed in a very clumpy manner, and that clumps are not self-shadowing. The strength of the signal received from many clumps in a single observing beam thus provides a measure for their total projected area weighted by brightness temperature. If the clumps are statistically similar from one line of sight to the other, we thus have a measure for the number of clumps per beam area, hence for the total amount of molecular material. In fact, the high optical depth of ^{12}CO emission is then a boon, as it makes such determinations to first approximation independent of the actual [CO]/[H₂] abundance.

1.2. Problems with CO-based methods

The most commonly used methods to estimate molecular hydrogen contents of extragalactic objects are either application of a 'standard' CO to H$_2$ conversion factor X (defined as the ratio of molecular hydrogen column density $N(H_2)$ to velocity-integrated CO intensity $I(CO)$) derived from Milky Way observations, or application of the virial theorem to observed CO clouds. The first method assumes similarity of extragalactic molecular clouds and Galactic clouds, or at least that the effects of different physical conditions cancel one another. In environments that are very different from those in the Galaxy, such as those found in galaxy central regions or in low-metallicity dwarf galaxies, this method must be considered unreliable (*cf.* Elmegreen et al. 1980; Israel 1988; Maloney & Black 1988; Elmegreen 1989; Maloney 1990a). For instance, application of this method to the very low CO luminosities commonly observed for irregular dwarf galaxies would suggest negligible amounts of H$_2$ (Israel et al. 1995) and consequently unusually high star formation efficiencies (Israel 1997). In contrast, direct evidence for X factors varying by more than an order of magnitude, probably as a function of local conditions, has been presented for Galactic clouds by Magnani & Onello (1995). We thus agree with Roberts & Haynes (1994): 'values of the molecular hydrogen content in late-type systems derived in this manner are uncertain and possibly too low by up to an order of magnitude'

The second method frequently used estimates total molecular cloud mass from observed parameters such as CO extent $R(CO)$ and velocity dispersion $dv(CO)$. Although this method, not assuming similarity between Galactic and extragalactic clouds, is preferable, it is likewise beset by problems, as it requires correct determination of the structure and dynamics of the observed clouds. For instance, the value of the virial constant used to convert observed parameters into mass may vary by a factor of four depending on the assumed condition of the system (see e.g. McLaren et al. 1988; McKee & Zweibel 1992), while it is not clear that the virial theorem is in fact relevant. If one considers the morphology of molecular complexes such as the ones in Orion (Bally et al. 1987), Taurus (Ungerechts & Thaddeus 1987) or indeed in the LMC (Israel & de Graauw 1991; Kutner et al. 1997) it is hard to imagine that these very elongated structures with little systematic velocity structure actually represent virialized complexes. Maloney (1990b) has shown that the correlation between CO luminosities and virial masses of Galactic molecular clouds follows directly from the size-linewidth relationship exhibited by molecular clouds and does not require virial equilibrium at all. Molecular hydrogen masses have also been determined applying X-factors scaled from X_{Gal} by $L(CO)$ as a function of dv (e.g. LMC – Cohen et al. 1988; SMC – Rubio et al. 1991).

Especially in the large linear beamsizes typical of extragalactic observations, actually unrelated clouds at somewhat different velocities may blend together, leading to unrealistical values of both cloud complex radius R and velocity dispersion dv. The derived (virial) masses may then either overestimate

or underestimate the actual mass, depending on circumstances. For instance, consider an area mapped with a large beam blending together N unrelated clouds, each having a true mass $M_{vir} = a\, r\, dv_o^2$. Here, r_o is the diameter of a single cloud and dv_o its velocity dispersion. The true total mass is thus $N\, a\, r_o\, dv_o^2$. Cloud emission is measured over an area with radius $R = N^{1/2}\, b\, r_o$ in which $b\, r_o$ is the projected separation between cloud centers. Unjustified application of the virial theorem on this observation suggests a total mass $M_{vir} = a\, N^{1/2}\, b\, r_o\, dv_1^2$, where dv_1 now is the dispersion derived from the velocity width of the sum profile of all clouds within radius R. The ratio of the derived mass over the true mass is thus:

$$M_{derived}/M_{true} = b\, N^{-1/2}\, (dv_1/dv_o)^2 \qquad (1)$$

If $N < b^2$ and $dv_1 > dv_o$, this will result in a potentially large overestimate of the mass. However, if instead the unrelated clouds are at more or less identical radial velocities, $dv_1 \approx dv_o$, the true mass is underestimated if $N > b^2$. Such a situation may occur in low-metallicity dwarf galaxies with relatively small velocity gradients. It occurs if we have a large number of clouds with small projected distances; a more physical equivalent is a very filamentary structure of the molecular material.

A further problem in estimating H$_2$ masses from CO observations is the need to assume virtually identical distributions for both. If CO is significantly depleted, H$_2$ may well occur outside the area delineated by CO emission and its amount is underestimated by the CO measurements. This effect appears to lie at the base of the size dependence of $N(H_2)/I(CO)$ ratio, noted by Rubio et al. (1993) and Verter & Hodge (1995). In low-metallicity galaxies suffering CO depletion, this results in a lack of CO emission in complexes observed on large angular scales. Observations on small angular scales selectively concentrate on the densest molecular components, that have resisted CO depletion most effectively, so that the $N(H_2)/I(CO)$ ratio looks progressively more 'normal' notwithstanding the lack of CO in *most* of the complex.

Thus, in order to estimate H$_2$ content of such galaxies, it is desirable to use a method that does not require specific assumptions on or knowledge of the detailed structure and dynamics of the molecular clouds involved. Use of far-infrared data in principle provides such a method (e.g. Thronson et al. 1987, 1988; Israel 1997).

2. Method and data

2.1. Estimating $N(H_2)$ from σ_{FIR} and $N(HI)$

H$_2$ column densities are derived in the manner used on NGC 6822 by Israel 1997. At locations well away from star-forming regions and CO clouds, the ratio of neutral hydrogen column density to far-infrared surface brightness $(N(HI)/\sigma_{FIR})_o$ is determined. In the absence of molecular gas, $(N(HI)/\sigma_{FIR})_o$ equals N_H/σ_{FIR}, which is a measure for the ambient gas-to-dust ratio. The observed σ_{FIR} values at locations that contain H$_2$, as betrayed by CO emission, reduced to the reference dust temperature T_{do} and then multiplied by $(N(HI)/\sigma_{FIR})_o$ thus provide the

total hydrogen column density N_H. The actual gas-to-dust ratio, which depends on poorly known dust particle properties, does not need to be known as long as it does not change from source to reference position. In the small irregular galaxies considered here, abundance gradients are negligible (cf. Vila-Costas & Edmunds 1992), so that we may safely assume no change in gas-to-dust ratio as a function of position in the galaxy. When N_H is known, $N(H_2)$ is found by subtracting the local $N(HI)$ value:

$$2 N(H_2) = [(N(HI)/\sigma_{FIR})_o f(T)\ \sigma_{FIR}] - N(HI) \qquad (2)$$

In Eq. 2, $f(T)$ is a function which corrects σ_{FIR} for the emissivity difference due to the (generally small) difference of T_d from T_{do}; for small temperature differences $f(T)$ is close to $(T_{do}/T_d)^6$. Temperatures T_d are derived from the IRAS $60\mu m/100\mu m$ flux ratio assuming a wavelength dependence for emission $I_\lambda \propto \lambda^{-n} B_\lambda$. Here and in the following we will assume n = 2. The temperature correction assumes that the number distribution of dust particles emitting at varying temperatures does not differ significantly from one location to another. This is a reasonable assumption for values of $f(T)$ not too far from unity, but may introduce significant errors for very large or very small values of $f(T)$. The CO to H₂ conversion factor X follows from the observed CO strength: $X = N(H_2)/I(CO)$.

This method of estimating H₂ column densities depends on observed quantities *independent of the actual spatial or kinematical distribution of the molecular material*. It has this property in common with the methods used by Bloemen et al. (1986) and Bloemen et al. (1990) to estimate the same quantities in the Milky Way galaxy. It avoids the major weakness of the virial method discussed above, as there is no need to determine the structure of the molecular cloud complexes, to separate unrelated clouds in the same line of sight, or even to resolve the molecular clouds. It is important to emphasize that in this method, the absolute gas-to-dust ratio plays no role, nor does the actual dust mass. We thus avoid a major uncertainty associated with other infrared-derived H₂ estimates, where the infrared flux is used to calculate a dust mass, which is then converted into a gas mass. Likewise, our results are independent of CO measurements, and as we will show below, the observational uncertainties are no worse than those associated with the traditional methods and probably better.

The column densities $N(H_2)$, and consequently X, determined in this paper are properly lower limits (Israel 1997). *(i)*. If some H₂ were to be present at the null positions where we assumed none, the total hydrogen column density corresponding to unit infrared luminosity is underestimated, implying higher actual $N(H_2)$ values than derived. *(ii)*. If, unexpectedly, the *hotter* infrared sources were to be relatively rich in *cooler* dust, the observed infrared emission does not sample the total amount of gas, hence $N(H_2)$, will be higher than estimated. *(iii)*. If, in regions of bright infrared emission, higher radiation densities would cause increased dust depletion, these regions will be characterized by a higher gas-to-dust ratio than assumed, again leading to higher than derived actual $N(H_2)$ values. This is ex-

pected only to be important for HII regions filling a significant fraction of the beam.

Errors in the assumptions would thus cause $N(H_2)$ and X to be higher rather than lower. Although these errors are hard to quantify, we consider it unlikely that their effect will exceed a factor of two. The calculated total hydrogen column densities N_H carry with them the combined uncertainty in the determinations of $(N(HI)/\sigma_{FIR})_o$, $f(T)$ and σ_{FIR}. Because these quantities are compared in a relative rather than an absolute sense, the uncertainty ΔN_H is of the order of 20% - 30% for the cases discussed below. The uncertainty in the calculated values of $N(H_2)$ is larger. Since the $N(HI)$ determinations are considered to be rather accurate, it depends on the molecular to atomic hydrogen ratio: $\Delta N(H_2) = \Delta N_H(1 + 0.5\ N(HI)/N(H_2))$

Thus, for H₂ column densities equal to or higher than those observed in HI, the relative H₂ uncertainty is typically less than 50%. For HI column densities substantially higher than the derived H₂ column density, the relative uncertainty may become considerable. However, this situation almost exclusively occurs at low absolute N(H₂) values where a relatively large uncertainty still corresponds to an acceptable uncertainty in the absolute value. The uncertainty in the derived value of X, in turn, includes both the uncertainty in $N(H_2)$ and in $I(CO)$. Since the latter is usually much smaller than the former, the uncertainty in X is actually dominated by that in $N(H_2)$. The combined effect of uncertainties in the observational values and in the assumptions implies a rough overall uncertainty of about a factor of two for individual determinations.

2.2. Data and results

All data were taken from the literature or existing databases. The CO, HI and far-infrared data included in the comparison are selected to have similar resolutions. This resolution is determined by the lowermost resolution to which the other data are degraded, if necessary.

2.2.1. LMC

The far-infrared data are from Schwering 1988, who conveniently produced maps of infrared luminosity over HI mass at 15′ resolution (corresponding to 235 pc) and dust temperature at 8′ resolution (Fig. 1). The HI data (resolution 15′) are from Rohlfs et al. (1984). The average of six positions in the main body of the LMC, well away from CO clouds and bright HII regions is $(N(HI)/\sigma_{FIR})_o = 2.25\times10^{27}$ cm⁻²/Wm⁻²sr⁻¹ (corresponding to $L/M = 1.7\ L\odot/M\odot$) at a reference temperature $T_{do} = 25.5$ K. From the internal variation, we estimate its uncertainty to be about 10%. The uncertainty in $f(T)$ is about 20% and that in σ_{FIR} about 10%.

In Table 1 we have listed data for several of the CO cloud complexes detected by Cohen et al. (1988) convolved to a resolution of 15′ (e.g. Meinert, 1992). Except for cloud 31, all CO clouds considered have diameters larger than 15′). Weaker CO sources are included only if identification with an HII re-

Table 1. LMC data (unit area 0.043 kpc^2)

CO Cloud	σ_{FIR} 10^{-6} $Wm^{-2}sr^{-1}$	$f(T)$	$N(HI)$ 10^{21} cm^{-2}	$N(H_2)$	$\frac{2N(H2)}{N(HI)}$	$\frac{2N(H2)}{N_{gas}}$	$I(CO)^a$ $Kkms^{-1}$	$X = \frac{N(H2)}{I(CO)}$ 10^{21} $cm^{-2}/Kkms^{-1}$	$\frac{\sigma_{FIR}}{N_H}$ [b] 10^{-28} $Wm^{-2}sr^{-1}cm^2$	Associated HII Region [c]
3	6.0	0.38	0.7	2.6±0.7	7.4	0.65	0.75	3.4±1.1	10.3	N83B
6	12	0.26	1.5	2.4±0.8	3.2	0.56	1.15	2.1±0.9	17.2	N11
6	1.2	1.00	1.2	0.8±0.3	1.3	0.42	1.35	0.6±0.2	4.4	N11-North
11	1.2	1.00	1.1	0.8±0.3	1.5	0.44	0.75	1.1±0.7	4.5	(Bar)
13	4.8	0.38	1.3	1.4±0.5	2.1	0.51	0.75	1.9±0.9	11.7	N105A
15	2.4	0.57	1.0	1.0±0.4	2.0	0.49	1.15	1.0±0.5	7.8	N113
–	1.8	0.57	1.2	0.6±0.3	1.0	0.37	0.40	1.4±1.1	7.8	N30
18	2.1	1.00	0.9	1.9±0.6	4.2	0.60	1.15	1.6±0.6	4.5	(Bar)
19	12	0.31	2.0	3.2±1.0	3.2	0.56	2.50	1.3±0.4	14.3	N44
20	1.8	0.51	1.5	0.3±0.3	0.4	0.21	1.15	0.3±0.3	8.7	N18/N144
22	1.2	0.57	0.7	0.4±0.2	1.1	0.40	0.75	0.6±0.3	7.8	N132
23	3.6	0.38	1.5	0.8±0.4	1.1	0.38	1.50	0.5±0.3	11.7	N48
26	4.2	0.38	1.0	1.3±0.4	2.6	0.53	0.40	3.3±1.8	11.7	N206
27	2.4	0.51	1.6	0.6±0.3	0.8	0.32	1.15	0.5±0.3	8.7	N148/N150
29	4.5	0.38	1.1	1.4±0.5	2.6	0.53	0.40	3.6±1.9	11.7	N57
31	1.8	0.57	1.0	0.7±0.3	1.4	0.43	0.40	1.6±1.2	7.8	N64
32	120	0.08	3.2	9.7±2.7	6.1	0.64	1.15	8.4±2.9	52.9	30 Dor
32^d	9.0	0.26	2.5	1.4±0.6	1.1	0.39	1.50	0.9±0.4	17.1	N157B
33^d	12	0.26	3.2	1.9±0.8	1.2	0.40	4.00	0.5±0.3	17.1	N159
34	1.2	1.20	3.0	0.1±0.4	0.1	0.05	0.55	0.2±0.6	1.9	N214
35	3.6	1.00	3.5	2.3±1.0	1.3	0.44	4.50	0.5±0.2	5.1	N176
36	1.8	1.45	3.0	1.4±0.7	0.9	0.36	2.30	0.6±0.3	3.1	N216
37	4.8	0.57	3.0	1.6±0.7	1.1	0.38	2.60	0.6±0.3	7.8	N167
Mean^e	4.3	0.61	1.7	1.3±0.2	1.9	0.42	1.40	1.3±0.2	9.2±1.0	—

^{a} Uncertainty in $I(CO)$ is 0.24 Kkms^{-1} (Cohen et al. 1988);
^{b} Uncertainty in $\frac{\sigma_{FIR}}{N_H}$ is 25%; c. Henize 1956;
^{d} Data unreliable because of location on strong emission gradients.
^{e} Mean values excluding 30 Doradus.

gion complex support their validity. In Table 1, the first column identifies the CO cloud by its number in Table 1 of Cohen et al. (1988). Column 2 lists the far-infrared surface brightness at the peak CO position, column 3 the value of $f(T)$ based on the dust temperature derived from the F_{60}/F_{100} flux ratio and column 4 the HI column density. Column 5 gives the molecular hydrogen column density calculated according to Eq. 2, while columns 6 and 7 give the resulting ratios of molecular hydrogen to atomic hydrogen and total gas (including helium) respectively. Column 8 gives the integrated CO intensity and column 9 the resulting value of X. In column 10 we give the ratio of the observed infrared surface brightness (*not* reduced in temperature) over total hydrogen column density $N_H = 2N(H_2) + N(HI)$. This ratio is a measure of the ambient radiation field strength per H nucleon. Finally, column 11 lists HII region(s) associated with the molecular cloud. In most cases the HII region extent is much less than the 15′ scale relevant to the data used.

Some further comments are in order. Clouds 34, 35 and 36 are located south of the bright HII regions associated with the Doradus complex. Major CO emission occurs with little or no optical counterpart. There is relatively strong HI emission,

but the far-infrared surface brightness decreases smoothly. The results for N157B and N159 (clouds 32 and 33) are uncertain, as both are at steep far-infrared gradients. N159 is also on a steep CO emission gradient in the opposite direction. Consequently, the resulting value of $N(H_2)$ depends critically on the precise (within a fraction of the resolution) position used. The *mean* value of the CO to H_2 conversion ratio (excluding 30 Doradus) is $X = 13(\pm2)\times 10^{20}cm^{-2}$. Its uncertainty is determined by that in $(N(HI)/\sigma_{FIR})_o$, which does not decrease with increasing sample size, whereas all other errors do.

2.2.2. SMC

The far-infrared data are from Schwering's (1988) maps of dust temperature and of far-infrared luminosity over HI mass (Fig. 2). The HI data at the same resolution are from McGee & Newton (1981). For the SMC we find an average $(N(HI)/\sigma_{FIR})_o = 1.65(\pm0.25)\times10^{28}$ cm$^{-2}/$Wm^{-2}sr^{-1} (corresponding to $L/M = 0.23$ $L\odot/M\odot$) for various positions in and near the bar, at a reference temperature $T_{do} = 28$ K. In Table 2 we list the SMC data for several of the CO cloud complexes detected by Rubio et al. (1991) in the same format as Table 1.

Table 2. SMC data (unit area 0.061 kpc^2)

CO Cloud	σ_{FIR} 10^{-6} Wm^{-2}sr^{-1}	$f(T)$	$N(HI)$ 10^{21}	$N(H_2)$ cm^{-2}	$\frac{2\,N(H2)}{N(HI)}$	$\frac{2\,N(H2)}{N_{gas}}$	$I(CO)$[a] Kkms^{-1}	$X = \frac{N(H2)}{I(CO)}$ 10^{21} cm^{-2}/ Kkms^{-1}	$\frac{\sigma_{FIR}}{N_H}$ [b] 10^{-28} Wm^{-2}sr^{-1}cm^2	Associated HII Region [c]
SW1	1.5	0.74	7.8	6.3±2.8	1.6	0.46	0.42	15±7	0.7	N16/N17
SW2	1.3	0.67	8.8	3.6±2.1	0.8	0.33	0.36	10±6	0.8	N25/N26
-	1.5	0.55	7.0	4.2±2.1	1.2	0.40	0.20	20±12	1.0	N32/N37
NE1	0.3	0.90	3.0	1.3±0.8	0.9	0.34	0.20	7±4	0.6	N72
NE2	1.3	0.55	4.3	4.4±1.8	2.1	0.50	0.33	13±6	1.0	N66
NE3	0.9	0.67	5.9	2.5±1.5	0.9	0.34	0.30	8±5	0.8	N76
Mean	1.1	0.68	6.1	3.7±0.8	1.3	0.40	0.30	12±2	0.8±0.1	—

[a] Uncertainty in $I(CO)$ is 0.06 Kkms^{-1} (Rubio et al. 1991);
[b] Uncertainty in $\frac{\sigma_{FIR}}{N_H}$ is 25%;
[c] Henize 1956.

Table 3. Other galaxies

Galaxy	σ_{FIR} 10^{-6} Wm^{-2}sr^{-1}	$f(T)$	$N(HI)$ 10^{21}	$N(H_2)$ cm^{-2}	$\frac{2\,N(H2)}{N(HI)}$	$\frac{2\,N(H2)}{N_{gas}}$	$I(CO)$[a] Kkms^{-1}	$X = \frac{N(H2)}{I(CO)}$ 10^{21} cm^{-2}/ Kkms^{-1}	$\frac{\sigma_{FIR}}{N_H}$ 10^{-28} Wm^{-2}sr^{-1}cm^2	Unit Area kpc^2
NGC 55	20	1.0	8.0	6.0±3.0	1.5	0.44	2.0	3.0±1.7	10±2	0.6
NGC 1569	12	1.5	3.5	6.0±3.0	3.4	0.57	0.37	16±8	8±2	0.7
NGC 4214	7	0.9	1.6	2.3±0.9	2.9	0.55	0.7	3.3±1.5	12±2	4.2
NGC 4449	1.6	0.45	1.85	0.7±0.3	0.6	0.28	0.95	8.0±3.0	2.3±0.6	2.1
NGC 6822-HII	0.85	0.7	1.8	2.8±0.9	3.1	0.56	0.50	5.5±1.1	1.1±0.2	0.1
NGC 6822-IR	0.75	0.8	1.5	3.0±0.5	4.0	0.59	0.85	4.7±1.3	1.0±0.2	0.1
NGC 604	2.0	0.6	3.0	2.6±1.0	1.7	0.47	1.2	2.2±0.9	2.4±0.5	0.5
NGC 595	1.1	1.0	1.9	1.0±0.4	1.1	0.38	0.9	1.2±0.9	2.7±0.6	0.5
NGC 5461	6	1.0	1.6	2.7±0.9	3.4	0.57	2.5	1.1±0.4	8±2	3.4

[a] For CO details, see text.

The *mean* value of the CO to H₂ conversion ratio is $X = 120(\pm30)\times10^{20}$cm^{-2}. The uncertainty in the null determination again dominates, but less decisively because of the relatively small sample size in Table 2.

2.2.3. NGC 55, NGC 1569, NGC 4214 and NGC 4449

Four other irregular galaxies have far-infrared, HI and CO data at similar resolutions (Table 3). For these galaxies, we used far-infrared data at a resolution of 1.4′ obtained with IRAS CPC instrument at 50μm and 100μm (F. Sloff, unpublished; Van Driel et al. 1993). For consistency, we interpolated the CPC 50μm fluxes to 60μm; as the absolute calibration of the CPC is unreliable (Van Driel et al. 1993), we scaled all CPC fluxes by the IRAS survey fluxes. In the case of NGC 55 we verified the outcome by comparison with the IRAS survey image-sharpening (PME) result published by Bontekoe et al. (1994).

NGC 55 was sampled at the CO cloud detected by Dettmar & Heithausen (1989) and at two reference positions 1.5′ on either side of this peak. Using HI data from Hummel et al. (1986), we found for the reference value $(N(HI)/\sigma_{FIR})_o = 1.4\pm0.2\times10^{28}$

cm^{-2}/Wm^{-2}sr^{-1}. Dettmar & Heithausen (1989) give a CO surface brightness of 3 Kkms^{-1} and a source size of $100''\times40''$, so that $I(CO) = 2$ Kkms^{-1} in a 1′ beam.

NGC 1569 was observed in CO by Greve et al. (1996) who detected a cloud with a peak $I(CO) = 2.9$ Kkms^{-1} and a size of 22″, corresponding to a CO intensity of 0.37 Kkms^{-1} in a 1′ beam. HI data at 1′ resolution are from J. Stil (private communication; see also Israel & Van Driel 1990). At the reference position 1.2′ to the southeast, where Greve et al. (1996) did not find CO emission, we determined $(N(HI)/\sigma_{FIR})_o = 7.7\times10^{28}$ cm^{-2}/Wm^{-2}sr^{-1}. Infrared emission gradients render this result uncertain by 25%. As weak CO emission might be present outside the limited area mapped, the uncertainty in X may be as high as 65%. If we take the Young et al. (1984) results ($I(CO) = 1.1\pm0.3$ Kkms^{-1} in a 50″ beam), we would find an X-ratio only half the value in Table 3, which we take as indicative of the uncertainty in X.

NGC 4214 was observed in CO by Becker et al. (1995) who found a cloud complex of dimensions $36''\times22''$ with a peak $I(CO) = 2.8$ Kkms^{-1} in a 21″ beam. After correction for beam-size, this is consistent with earlier and less accurate determina-
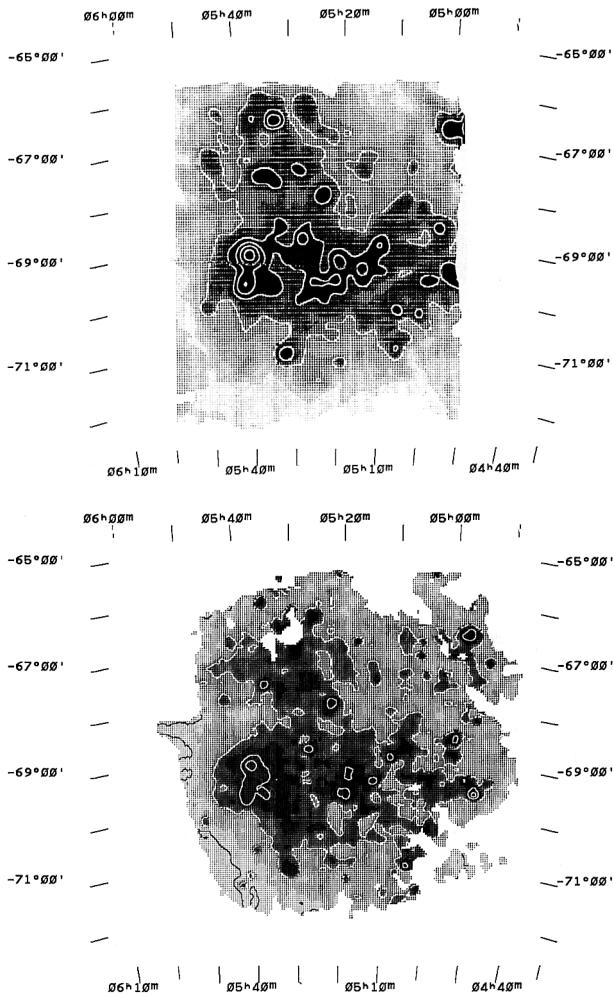
Fig. 1. LMC. Top: ratio of far-infrared luminosity to neutral hydrogen column density at 15′ resolution. Contours are at 5.3, 13, 26, 52, 105 × 10^{-28} W m^{-2} sr^{-1} cm^2. Bottom: dust temperature T_d at 8′ resolution. Contours are at 23, 28, 32 and 36 K.
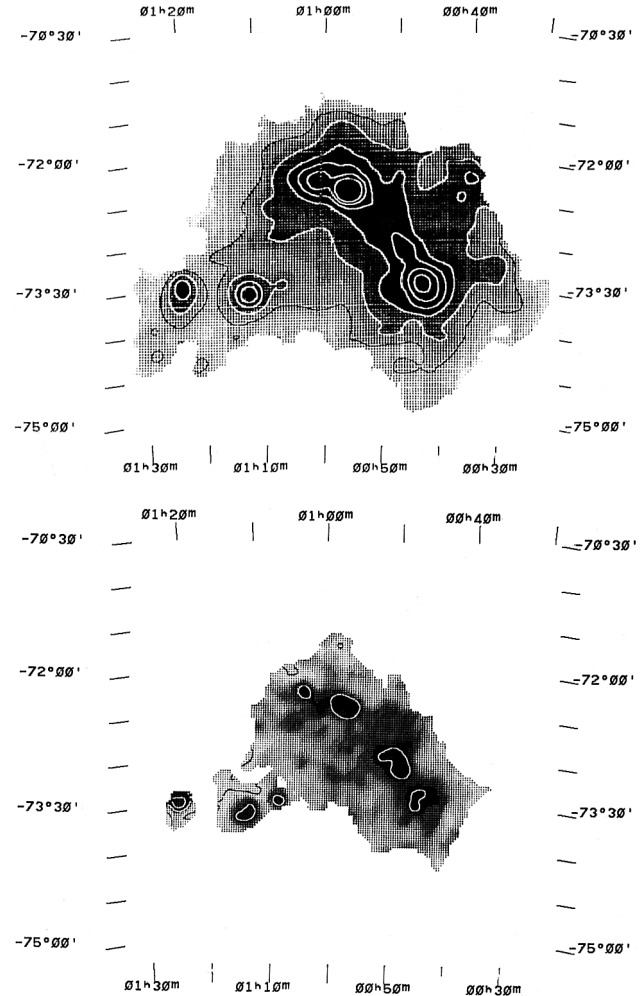

Fig. 2. SMC. Top: ratio of far-infrared luminosity to neutral hydrogen column density at 15′ resolution. Contours are at 2.6, 5.2, 10.5, 15.7, 21, 26 × 10^{-29} W m^{-2} sr^{-1} cm^2. Bottom: dust temperature T_d at 8′ resolution. Contours are at 28, 32 and 36 K.

tions by Tacconi & Young (1985) and Thronson et al. (1988). Weak CO was also detected by Ohta et al. (1993) in a 15″ beam towards positions 45″ southeast and 35″ northwest of the reference position given by Becker et al. (1995). On the basis of all available data, we take $I(CO) = 0.7(\pm0.15)$ Kkms^{-1} in a 1′ beam. HI data at 1′ resolution are from Allsop (1979). At two reference positions, we determined $(N(HI)/\sigma_{\mathrm{FIR}})_o = 1.2\pm0.2\times10^{27}$ cm^{-2}/Wm^{-2}sr^{-1}.

NGC 4449 was observed in CO by Hunter & Thronson 1996 (65″ beam) and by Sasaki et al. 1990 (15″ beam). Taking into account beam sizes and efficiencies, the data agree well. HI data at 1′ resolution are from the WHISP database (J. Kamphuis, private communication). We obtained reasonably accurate infrared surface brightnesses for Hunter & Thronson's regions 1 through 4 only and determined $(N(HI)/\sigma_{\mathrm{FIR}})_o = 4.35\pm1.0\times10^{27}$ cm^{-2}/Wm^{-2}sr^{-1}. Table 3 gives the mean of the individual results for the four positions, weighted by *I(CO)*.

2.2.4. Extragalactic HII regions

In Table 3, we have also included the results obtained for NGC 6822 (Israel 1997). Two sets of entries are given: NGC 6822-HII represents the mean values towards the HII region complexes Hubble I/III, V and X, and NGC 6822-IR those towards the infrared sources 4 and 6 not associated with major HII regions.

We also included data for the bright HII regions NGC 604 and NGC 595 in M 33. The infrared data were taken from Rice et al. (1990), HI data at the same resolution from Deul (1988) and CO data from Blitz (1985). Note that the results for NGC 595 are rather uncertain, as a reliable flux at 100μm is hard to determine; we assumed essentially similar infrared flux distribtions for both NGC 604 and NGC 595. Finally, we also included NGC 5461, the brightest HII region in the galaxy M 101. Infrared data were taken from Bontekoe et al. (1994), HI data from van der Hulst & Sancisi (1988) and CO data from Blitz et al. (1981) and Kenney et al. (1991). In this case, we applied a correction factor of 1.3 to allow for the presence of significant amounts of HII; this effect

is negligible for the M 33 objects. Because the parent galaxies M 33 and M 101 have radial abundance gradients, we selected null positions adjacent to the HII regions used.

3. Analysis and discussion

3.1. The CO to H_2 conversion factor

In the sample galaxies, we find CO to H_2 conversion factor X values much higher than the range $0.2\text{-}0.4 \times 10^{21}$ cm^{-2} (Kkms^{-1})$^{-1}$ commonly adopted for Milky Way objects. In the LMC, we find a mean value $X = 1.3 \times 10^{21}$ cm^{-2} (Kkms^{-1})$^{-1}$, or 3 - 7 times higher than in the Milky Way. We may compare this result to that obtained by Cohen et al. (1988). Comparing CO luminosities $L(CO)$ to velocity width Δv, they conclude that on average $X_{\mathrm{LMC}} = 6X_{\mathrm{G}}$. They adopt $X_{\mathrm{G}} = 0.28 \times 10^{21}$ cm^{-2} (Kkms^{-1})$^{-1}$ resulting in a value for X_{LMC} 30% higher than ours. However, if $X_{\mathrm{G}} = 0.20 \times 10^{21}$ cm^{-2} (Kkms^{-1})$^{-1}$ (Bloemen 1989), their result is identical to ours. Satisfactory as this may seem, the situation is more complex.

First, Cohen et al. (1988) estimated their value of X from the mean ratio $L(CO)_{\mathrm{G}}/L(CO)_{\mathrm{LMC}}$, but their Fig. 2 shows this ratio to be a function of Δv. At the smallest velocity widths, their implied X_{LMC} is only 3 X_{G}, but at the largest widths it is $10X_{\mathrm{G}}$. The figure exhibits a large scatter around the mean, covering an equivalent range in X_{LMC} of 2 - 20 X_{G}. Part of this scatter is undoubtedly due to the low signal-to-noise ratio of the CO measurements, but part of it is real. For instance, Garay et al. (1993) studied seven CO clouds in the 30 Doradus halo and found those to have $L(CO)_{\mathrm{G}}/L(CO)_{\mathrm{Dor}}$ ratios implying a much higher value $X_{\mathrm{Dor}} = 20 X_{\mathrm{G}}$ than the mean found by Cohen et al. (1988). We note that the values tabulated in our Table 2 also define a large range in X, from close to the Galactic value to more than an order of magnitude higher. For 30 Doradus itself we derive an even higher X value. We will discuss this variation in X in Sect. 3.2.

Second, we differ in individual cases, even though the mean values agree. For instance, Cohen et al. (1988) obtain very high H_2 and virial masses (and their Fig. 2 implies a high value for X) in cloud 35. In this cloud, we find a *low X* value. The result by Cohen et al. (1988) follows from the high $\Delta v = 28$ km s^{-1} they found for this cloud. They list similarly large velocity widths for e.g. clouds 13, 19 and 23. Yet, the higher resolution SEST survey yields velocity widths typically a factor of two less (Israel et al. 1993; Kutner et al., 1997). At least in the case of cloud 35, the anomalously high velocity width appears to be the result of CO clouds at two distinct velocities blended together in the large beam used by Cohen et al. (1988). Reduction of the large velocity widths to the more modest SEST values, yields X values in much better agreement with those in Table 2. Similar comments apply to the SMC results by Rubio et al. (1991), except that here we find a *larger* value of X, although both results have significant uncertainties associated with them. It is nevertheless clear that X_{SMC} is much higher than either X_{LMC} or X_{G}.

Table 4. Comparison of X values

Galaxy	X 10^{21} cm^{-2}/ Kkms^{-1} This Paper	Literature	References
LMC	1.3	1.7; 3.9	1; 2
SMC	12	6	3
NGC 55	3	6	4
NGC 1569	16	5	5
NGC 4214	3	2; 1	6; 7
NGC 4449	0.8	1	8
NGC 6822	5	0.6–3	9
NGC 604	2.2	3; 0.35; 3.5	10; 11; 12; 13
NGC 595	1.2	1.4; 0.6	10; 12
NGC 5461	1.1	2	14

References for other X values: 1. Cohen et al.(1988); 2. Garay et al. (1993); 3. Rubio et al. (1991); 4. Dettmar & Heithausen (1989); 5. Greve et al. (1996); 6. Thronson et al. (1988); 7. Becker et al. (1995); 8. Estimated from Ohta et al. 1993, after correction for main-beam efficiency; 9. Wilson (1994); 10. Estimated from Blitz (1985); 11. Viallefond et al. (1992); 12. Wilson & Scoville (1992); 13. Israel et al. (1990); 14. Estimated from Blitz et al. (1981).

For the objects listed in Table 3, X estimates can be obtained from the literature (Table 4). These are mostly rough estimates based on comparison of CO luminosities and virial masses, and are very uncertain. Nevertheless, we see reasonably good agreement in Table 4 for NGC 55, NGC 4214, NGC 4449 and for NGC 5461. There is also good agreement for NGC 595 and NGC 604 if we disregard the estimates derived from the high resolution observations which apply to individual cloud components rather than whole complexes. It has been noted before (Rubio et al. 1993; Verter & Hodge, 1995) that such observations always yield X values much lower than the global values derived from observations covering the whole complex (see als Sect. 1.2). Our results for NGC 6822, and especially for NGC 1569, are higher than the other published estimates.

3.2. Dependence of X on environment

3.2.1. Dependence on radiation field

Compared to the Milky Way, the galaxies studied here have lower metallicities, and are found to have higher X ratios. This is not a new result: several authors have suggested a more or less inverse linear dependence between X and metallicity as measured by the oxygen abundance (*cf.* Dettmar & Heithausen, 1989; Rubio et al. 1991; Verter & Hodge 1995; Arimoto 1996, Sakamoto 1996). Arnault et al. (1988) found the ratio of CO to HI emission in a sample of 19 late-type galaxies to vary roughly as [O]/[H]$^{2.2}$. Sage et al. (1992) failed to reproduce such a relation, but our sample suggests the CO to HI ratio to be proportional to [O]/[H]$^{2.6}$, within the errors identical to the result obtained by Arnault et al. (1988). The latter conclude that CO must be deficient relative to H_2 as a function of metallicity, but could not determine a functional dependence for the CO/H_2 ratio, hence X, on metallicity. Their result nevertheless suggests
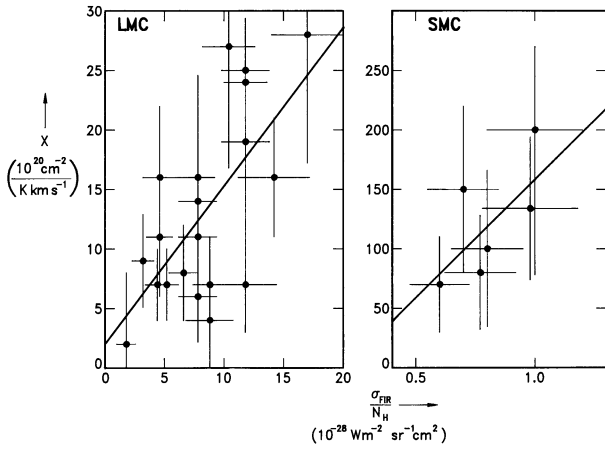
Fig. 3. Dependence of X on radiation field as represented by the ratio σ_{FIR}/N_H. Left: LMC; right SMC. Linear regression lines are plotted.

a dependence with a coefficient larger than unity, as there is no reason to assume vastly different H$_2$/HI ratios in low-metallicity galaxies. The present data provide an excellent basis to pursue this question, as they have been obtained in a consistent manner. Much of the previously published discussions were based on a compilation of data (notably X-values) from different sources, and obtained in different manners.

An underabundance of CO with respect to hydrogen is expected to result from low carbon and oxygen abundances. It will be enhanced by photodissociation of CO since low metal abundances imply both lower selfshielding and lower dust shielding of CO against the ambient radiation field. The LMC and SMC samples allow us to first investigate the effect of the radiation field. In Fig. 3 we have plotted the ratio $N(H_2)/I(CO) = X$ as a function of the energy available per H nucleon, represented by the quantity σ_{FIR}/N_H. Straight lines indicate the linear regression lines. In case of the LMC, we did not include 30 Doradus in determining the regression line, because its very high values would dominate the result. Nevertheless, extrapolation of the regression line to the σ_{FIR}/N_H value of 30 Doradus predicts it to have $X = 7 \times 10^{20}$cm^{-2} cm^{-2} (Kkms^{-1})$^{-1}$, or 85% of the value derived directly in Table 1. The SMC sample, although much smaller, shows a similar behaviour. Further analysis suggests that the dependence of X on radiation field is indeed very close to linear: $X \propto (\sigma_{FIR}/N_H)^{0.9\pm0.1}$.

The increase of X, i.e. the decrease of CO relative to $N(H_2)$, as more energy per nucleon is available is the result of two processes, as is illustrated by the SEST results obtained for the LMC. High-resolution maps (linear beamsize corresponding to 10 pc) were obtained of clouds 35/36 (south of 30 Doradus – Kutner et al. 1997), cloud 6 (N11 – see Israel & de Graauw 1991) and cloud 32 (30 Doradus – Johansson et al., in preparation). The map of cloud 35/36 shows numerous clumps embedded in extended interclump gas; the average peak-to-diffuse CO contrast ratio is about 3. Bright clumps (i.e. those having a CO strength of more than 5 Kkms^{-1} per SEST beam area) are numerous, but contribute only about a quarter to a third of the CO luminosity of the whole complex. This is similar to Galactic
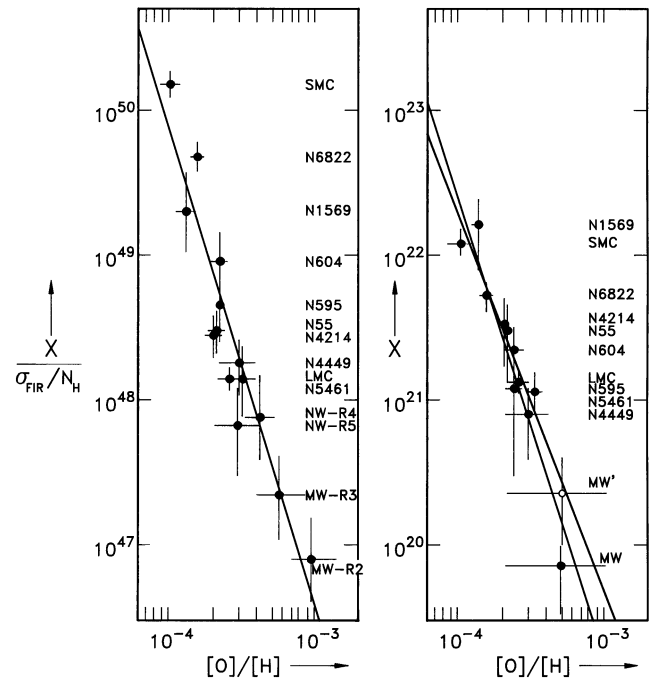

Fig. 4. Dependence of X on metallicity. a. At left: the ratio of X to σ_{FIR}/N_H as a function metallicity [O]/[H]. The linear regression is drawn as a solid line. Only one line is drawn, as inclusion of the Milky Way points does not perceptibly change the result. b. At right: X as a function of metallicity [O]/[H] regardless of ambient radiation field. Global Milky Way points are indicated corresponding to 'Y' from Bloemen at al.(1990 – filled circle) and the more commonly used 'X' from Bloemen et al. (1986 – open circle). Regression lines are marked for the sample galaxies only, and for the sample galaxies with the addition of the Galactic 'Y' point (steeper line).

giant molecular clouds, where e.g. Heyer et al. (1996) find most of the molecular mass to be in extended, low column-density regions. Cloud 6 is embedded in a four times stronger radiation field (Table 1) and contains a very similar number of clumps per unit area. Two thirds of these are bright with $I(CO) > 5$ Kkms^{-1} per SEST beam, but cloud 6 lacks the extended diffuse gas seen in cloud 35/36. In this complex, the contrast ratio is of order ten. Apparently, the fourfold increase in radiation density has resulted in the removal of virtually all the low column density CO gas. As the high column density hydrogen gas will be practically unaffected, the value of X has increased in cloud 6 more or less commensurate with the increase in radiation density and CO removal.

Cloud 32 experiences a radiation density a factor of three over that in cloud 6, i.e. over an order of magnitude more than that of Cloud 35/36. There is no trace of interclump gas. The number of clumps per unit area is still very similar, but the fraction of *bright* clumps is only a third, down by more a factor of two from Cloud 6. Many of the weaker clumps are hardly discernible. We conclude that the further increase in radiation density in cloud 32 is eroding even the dense CO clumps that are surviving reasonably well in cloud 6, resulting in a further decrease of the $I(CO)/N(H_2)$ ratio, i.e. a further increase in X.

It is of interest that the low-excitation clouds south of N 159 have X values only a few times 10^{20}cm^{-2} cm^{-2} rather similar to the canonical value of X in the Milky Way. In these clouds, the lack of dissociating radiation apparently allows the CO to fill most of the H$_2$ volume, nothwithstanding the lower CO abundance.

3.2.2. Dependence on metallicity

The ratio of X to σ_{FIR}/N_H for the objects in Tables 1, 2 and 3 can now be compared to the metallicities given in Table 5. We have included the Milky Way by using the Y and σ_{FIR}/N_H values tabulated as R2 tot R5 by Bloemen et al. (1990 – their Table 3) and the metallicities from Shaver et al. (1983). We have determined linear regressions with and without the Milky Way points, and for X–σ_{FIR}/N_H dependences with exponents 0.9 and 1.0. We find:

$\log X = 0.9\pm0.1 \log(\frac{\sigma_{FIR}}{N_H})$ - $3.5\pm0.2 \log\frac{[O]}{[H]}$ + 34.6 ± 2.2
($n = 10$; regression coefficient $r^2 = 0.78$)　　　　(3a)

Inclusion of the Milky Way points changes this to:

$\log X = 0.9\pm0.1 \log(\frac{\sigma_{FIR}}{N_H})$ - $3.2\pm0.1 \log\frac{[O]}{[H]}$ + 34.3 ± 3.1
($n = 14$; $r^2 = 0.85$)　　　　(3b)

This is illustrated in Fig. 4a, which shows the dependence on [O]/[H] for a linear (exponent 1.0) dependence of X on σ_{FIR}/N_H. As is clear from Fig. 4a, there is almost perfect agreement of the Milky Way points with the relation determined for the sample galaxies alone. We have also empirically determined the dependence of X on metallicity, ignoring any dependence on radiation density. This yields (see also Fig. 4):

$\log X = $ -$2.7\pm0.3 \log\frac{[O]}{[H]}$ + 11.6 ± 1.0
($n = 10$; $r^2 = 0.90$)　　　　(4)

Here, the nominal global Milky Way Y-point (Bloemen et al. 1990) is low compared to the relation defined by the sample galaxies, while the commonly used value $X = 2.3 \times 10^{20}$ cm^{-2}(Kkms^{-1})$^{-1}$ provides a very good fit.

The dependence of X on [O]/[H] alone, ignoring σ_{FIR}/N_H effects, found here is significantly steeper than the result $\log X \propto 1.5 \log$ [O]/[H] found by Sakamoto (1996) from modelling radiative transfer and excitation of CO in clumpy molecular clouds. However, that result did not take into account the full effects of photodissociation of CO especially on the interclump gas.

With respect to steep dependences on metallicity, we note that Garnett et al. (1995) have shown that [C]/[O] $\propto$ [O]/[H]$^{0.43\pm0.09}$, so that [C]/[H] should be proportional roughly to [O]/[H]$^{1.5}$. If the CO abundance is solely determined by the carbon abundance, [CO]/[H] likewise will be proportional to [O]/[H]$^{1.5}$; if the oxygen abundance plays a role this may increase to [O]/[H]$^{2.5}$. The strength of the radiation field experienced by CO is proportional to the photon flux diluted by dust extinction. To first order, we may equate the decrease in dust

Table 5. Adopted abundances

Galaxy	[O]/[H] 10^{-4}	References
LMC	2.60±0.40	1, 2, 3, 4
SMC	1.05±0.20	1, 2, 3, 4
NGC 55	2.15±0.25	5, 6, 7
NGC 1569	1.35±0.15	2, 5
NGC 4214	2.05±0.15	2, 7, 8
NGC 4449	3.0±1.0	2, 9, 10
NGC 6822	1.60±0.15	2, 5, 11, 12, 13
NGC 604	2.40±0.30	14, 15, 16
NGC 595	2.40±0.30	14, 16
NGC 5461	3.30±0.40	9, 17, 18

References for abundances: 1. Dufour (1984) and references cited; 2. Skillman et al. (1989a) and references cited; 3. Campbell (1992); 4. Pagel et al. (1992); 5. Talent (1980); 6. Webster & Smith 1983; 7. Stasinska et al. (1986); 8. Kobulnicky & Skillman 1996; 9. McCall (1982); 10. Hunter et al. (1982) 11. Skillman et al (1989b); 12. Kinman et al. (1979) 13. Pagel et al. (1980); 14. Kwitter & Aller (1981); 15. Diaz et al. (1987); 16. Vilchez et al. (1988); 17. Rayo et al. (1982); 18. Evans (1986).

shielding with the decrease in dust abundance. As the dust-to-gas ratio in galaxies is about proportional to [O]/[H] (see e.g. Issa et al. 1990), we expect photodissociation alone to gain in importance as roughly [O]/[H]$^{-3}$ when metallicity decreases. Because the effects of photo-dissociation are highly non-linear, and depend critically on the balance between ambient radiation field and local column densities, a more quantitative estimate of the effect of metallicity can only be obtained by detailed modelling, which should treat photodissociation more rigorously and take into account the structure and column density distribution of the molecular clouds experiencing the dissociating radiation (*cf.* Maloney 1990a). This is beyond the scope of this paper.

3.3. H$_2$ masses

The results given in Tables 1 and 2 show the presence of significant amounts of molecular hydrogen in both the LMC and the SMC. At the (CO-selected) positions sampled, H$_2$ locally dominates the interstellar gas. Table 3 suggests that this is also true in the other galaxies.

Can we extrapolate the results obtained so far to estimate the *total* amount of H$_2$ in the sample galaxies? Application of the mean X value from Table 1 to the LMC CO results obtained by Cohen et al. (1988) yield $M(H_2) = 0.8 \times 10^8$ $M_\odot$. A more detailed treatment, applying the individual $N(H_2)$ values from Table 1 to the cloud complex sizes given by Cohen et al. (1988) and correcting for their CO sources not included in our Table 1, yields a higher value $M(H_2) = 1.2 \times 10^8$ $M_\odot$. This result is very similar to that obtained by Cohen et al. (1988) (but see Sect. 3.1). It corresponds to a global mass ratio of molecular-to-atomic hydrogen of 0.2, much lower than the mass ratio of

Table 6. Global H$_2$ mass estimates

Galaxy	M(HI)	$M'_{\rm H}$	M(H$_2$)	$\frac{M(\rm H_2)}{M(\rm HI)}$	$\frac{M(\rm H_2)}{M_{\rm gas}}$
		$10^8\ M_\odot$			
LMC	5.4	1.1	1.0	0.19	0.12
SMC	5.0	1.8	0.75	0.20	0.12
NGC 55	18.6	4.8	2.9	0.16	0.10
NGC 1569	1.4	0.65	0.5	0.35	0.20
NGC 4214	11.2	1.4	1.0	0.09	0.06
NGC 4449	55	21	8.7	0.16	0.10
NGC 6822	1.5	0.5	0.4	0.27	0.16
Mean				0.20	0.12
				±0.04	±0.02
Milky Way	48	—	12	0.25	0.15

1.9 found for the *individual CO clouds* in Table 1. It implies that in the LMC, about 12% of all the interstellar gas, including helium, is in molecular form.

We have also applied Eq. (2) to the total *far-infrared* emission of the LMC, yielding a total hydrogen mass $M'_{\rm H} = 1.1 \times 10^8\ M_\odot$, much less than the observed total HI mass *M(HI)* = $5.4 \times 10^8\ M_\odot$ (McGee & Milton 1966). Apparently, the LMC contains a significant fraction of relatively cool dust not significantly contributing to the total infrared luminosity. However, we may still estimate the total amount of H$_2$ *associated with the warm dust* by assuming the mean H$_2$/HI mass ratio from Table 1 to apply to all sources of warm H$_2$: we then find $M(H_2)$ = $0.7 \times 10^8\ M_\odot$. This rougher method thus underestimates the actual amount of H$_2$ by about 30%.

Following the same procedures for the SMC, we find $M(H_2)$ = $0.50\pm0.05 \times 10^8\ M_\odot$, implying $M(H_2)/M(HI) = 0.1$, or 7% of all interstellar gas in molecular form. This is a lower limit, since the CO observations by Rubio et al. (1991) cover only part of the SMC. Indeed, extrapolation to the total infrared luminosity of the SMC yields $M'_{\rm H} = 1.75 \times 10^8\ M_\odot$ which nevertheless still falls short of the total HI mass *M(HI)* = $5 \times 10^8\ M_\odot$ (Hindman 1967). Applying the mean H$_2$/HI mass ratio from Table 2, we obtain $M(H_2) = 1.0 \times 10^8\ M_\odot$.

The galaxies listed in Table 3 were not sampled extensively in CO, so that we can only extrapolate from the total infrared luminosity. However, the example of the LMC suggests that this extrapolation is accurate to about 30%. The results are given in Table 6, which also includes the global results for the Milky Way given by Bloemen et al. (1990). Table 6 shows that molecular hydrogen, although dominating the interstellar medium near star formation regions, occurs much less predominantly in irregular dwarf galaxies as a whole. Globally, the total mass of atomic hydrogen is typically five times higher than that of molecular hydrogen. On average, about one eigth of the interstellar gas mass is in molecular form. These fractions are surprisingly close to those of the Milky Way Galaxy as a whole, where the fraction of molecular gas reaches a peak of 0.46 in the 'molecular ring' at R = 4 – 8 kpc, and drops to 0.11 in the outer galaxy (Bloemen et al. 1990). If $X_{\rm Gal}$ is somewhat lower than assumed by Bloemen et al., as has been suggested by e.g. Bhat et al. (1986),

the similarity of the Milky Way and irregular dwarf mean ratio is even more striking. Our result does not reproduce the apparent dependence of global molecular gas fraction on metallicity discussed by Tosi & Díaz (1990) and Vila-Costas & Edmunds (1992). We note that the latter expressed doubts on the physical significance of that result, and suggested that it might be an artifact of the CO to H$_2$ conversion used. Our result implies that this is indeed the case.

The molecular hydrogen fraction in this admittedly small sample appears to be uncorrelated with metallicity, hence presumably dust-to-gas ratio. This is somewhat surprising as H$_2$ molecules form on dust grain surfaces, so that one would expect less H$_2$ in low metallicity environments poor in dust grains. Our result may thus indicate that the formation of H$_2$ is so efficient, that it is to first order independent of the dust abundance. Alternatively, it may reflect a selection effect. Higher metallicity environments provide more shielding and therefore may have a larger fraction of cold dust/molecular hydrogen than lower metallicity environments. In the presence of warm dust, IRAS fluxes poorly sample cold dust, so that we may increasingly have underestimated the total amount of H$_2$ for the higher metallicity galaxies.

4. Conclusions

1. IRAS far-infrared surface brightnesses and HI column densities are used to indepently estimate H$_2$ column densities towards CO clouds observed in the LMC and SMC. Generally, in these clouds H$_2$ mass surface densities exceed those of HI by a factor of about 1.5 on average. This is in contrast to the global H$_2$ to HI mass ratios which are of the order of 20±10 %.

2. By combining the newly derived H$_2$ column densities with published CO intensities, the CO to H$_2$ conversion factors X are determined to be $X_{\rm LMC} = 1.3\pm0.2 \times 10^{21}$ molecules cm^{-2} (Kkms^{-1})$^{-1}$ and $X_{\rm SMC} = 12\pm2 \times 10^{21}$ molecules cm^{-2} (Kkms^{-1})$^{-1}$. The global mass of (warm) molecular hydrogen is estimated to be $M(H_2) = 1.0\pm0.3 \times 10^8\ M_\odot$ for both LMC and SMC.

3. On average somewhat higher molecular to atomic hydrogen mass surface densities are found in the irregular dwarf galaxies NGC 55, NGC 1569, NGC 4214, NGC 4449 and NGC 6822, as well as in the extragalactic HII region complexes NGC 604, NGC 595, both in M 33, and NGC 5461 in M 101. The X-values derived for the HII regions and NGC 4449 are comparable to that of the LMC, while the X-values derived for NGC 55, NGC 4214 and NGC 6822 are typically two to four times higher; NGC 1569 has a very high value comparable to that of the SMC.

4. Analysis suggests that the CO to H$_2$ conversion factor X is linearly dependent on the strength of the ambient radiation field per nucleon, and inversely dependent on a steep function of metallicity [O]/[H]: $\log X = 0.9\pm0.1 \log\frac{\sigma_{\rm FIR}}{N_{\rm H}}$ - $3.5\pm0.2 \log\frac{[O]}{[H]}$ + 34.6±2.2. If the dependence on radiation field is neglected, the relation $\log X = -2.7\pm0.3 \log\frac{[O]}{[H]}$

+ 11.6±1.0 also fits the data. Similarly derived Milky Way values fit these same relations. They are interpreted as the result of selective photodissociation of CO under conditions of high radiation field energy densities and poor shielding and selfshielding in low-metallicity environments. Thus, over the parameter range studied, the CO content of galaxies varies strongly as a function of conditions.

5. Estimates of the global (warm) H$_2$ to HI mass ratios and the (warm) H$_2$ gas fractions yield very similar results for all galaxies. On average, $M(H_2) = 0.20\,M(HI)$, and $M(H_2) = 0.12\,M_{gas}$. These ratios are very close to the global Milky Way ratios: the global warm H$_2$ fraction in irregular dwarf galaxies appears to be very similar to that of our Galaxy, notwithstanding the large differences in total mass, luminosity, metallicity and observed CO luminosity.

References

Allsop N.J., 1979 MNRAS 188, 765

Arimoto N., Sofue Y., Tsujimoto T., 1996 PASJ 48, 275

Arnault Ph., Casoli F., Combes F., Kunth D., 1988 A&A 205, 41

Bally J., Langer W.D., Stark A.A., Wilson R.D., 1987 ApJL 312, L45

Becker R., Henkel C., Bomans D.J., Wilson T.L., 1995 A&A 295, 302

Bhat C.L., Mayer C.J., Wolfendale A.W., 1986 Phil. Trans. R. Soc. Lond., 319, 249

Blitz L., 1985 ApJ 296, 481

Blitz L., Israel F.P., Neugebauer G., et al. 1981 ApJ 249, 76

Bloemen J.B.G.M., Strong A.W., Blitz L., et al., 1986 A&A 154, 25

Bloemen J.B.G.M., 1989 in Physics and Chemistry of Interstellar Molecular Clouds, Eds. G. Winnewisser & J.T. Armstrong (Berlin: Springer), p. 22

Bloemen J.B.G.M., Deul E.R., Thaddeus P., 1990 A&A 233, 437

Bontekoe Tj. R., Koper E., Kester D.J.M., 1994 A&A 284, 1037

Campbell A., 1992 ApJ 401, 157

Cohen R.S., Dame T.M., Garay G. et al., ApJL 331, L95

Dettmar R.-J., Heithausen A., 1989 ApJL 344, L61

Deul E.R., 1988 Ph.D. Thesis, University of Leiden (NL)

Diaz A.I., Terlevich E., Pagel B.E.J., Vilchez J.M., Edmunds M.G., 1987 MNRAS 226, 19

Dufour R.J., 1984 in Structure and Evolution of the Magellanic Clouds, IAU Symp. 108, Eds. S. van den Bergh and K.S. de Boer (Dordrecht: Kluwer), p. 353

Eddington A.S., 1937 Observatory 60, 99

Elmegreen B.G., 1989 ApJ 338, 178

Elmegreen B.G., Elmegreen D.M., Morris M., 1980 ApJ 240, 455

Evans I.N., 1986 ApJ 309, 544

Garay G., Rubio M., Ramírez S., Johansson L.E.B., Thaddeus P., 1993 A&A 274, 743

Garnett D.R., Skillman E.D., Dufour R.J. et al., 1995 ApJ 443, 64

Gould R.J., Salpeter E.E., 1963 ApJ 138, 393

Greve A., Becker R., Johansson L.E.B., McKeith C.D., 1996 A&A 312, 391

Henize K., 1956 ApJS 2, 315

Heyer M.H., Carpenter J.M., Ladd E.F., 1996 ApJ 463, 630

Hindman J.V., 1986 Ast. J. Phys 20, 147

Hollenbach D.J., Werner M.W., Salpeter E.E., 1971 ApJ 163, 165

Hummel E., Dettmar R.-J., Wielebinski R., 1986 A&A 166, 97

Hunter D.A., Gallagher J.S., Rautenkranz D., 1982 ApJS 49, 53

Hunter D.A., Thronson H.A., 1996 ApJ 461, 202

Israel F.P., 1988 in: Millimetre and Submillimetre Astronomy, eds. R.D. Wollstencroft & W.B. Burton (Kluwer: Dordrecht), p. 281

Israel F.P., 1997 A&A 317, 65

Israel F.P., van Driel W., 1990 A&A 236, 323

Israel F.P., de Graauw Th. 1991 in: The Magellanic Clouds, Eds. R.F. Haynes & D. Milne (Kluwer: Dordrecht), p. 45

Israel F.P., Hawarden T.G., Geballe T.R., Wade R., 1990 MNRAS 242, 471

Israel F.P., Johansson L.E.B., Lequeux J., et al. 1993 A&A 276, 25

Israel F.P., Tacconi L.J., Baas F., 1995 A&A 295, 599

Issa M.R., McLaren I., Wolfendale A.W., 1990 A&A 236, 237

Kenney J.D.P., Scoville N.Z., Wilson C.D., 1991 ApJ 366, 432

Kinman T.D., Green J.R., Mahaffey 1979 PASP 91, 749

Kobulnicky H.A., Skillman E.D., 1996 ApJ 471, 211

Kutner M., Rubio M., Booth R.S., et al. 1997 A&AS 122, 255

Kwitter K.B., Aller L.H., 1981 MNRAS 195, 939

Magnani L., Onello J.S., 1995 ApJ 443, 169

Maloney P.R., 1990a in The Interstellar Medium in Galaxies, Eds. H.A. Thronson & J.M. Shull, (Dordrecht: Kluwer), p. 493.

Maloney P.R., 1990b ApJL 348, L9

Maloney P.R., Black J.H., 1988 ApJ 325, 389

McCall M.L., 1982 The Chemistry of Galaxies, Univ. Texas Publ. in Astronomy No. 20

McGee R.X., Milton J.A., 1966, Aust. J. Phys. 19, 343

McGee R.X., Newton L.M., 1981, Proc. astr. Soc. Aust. 4, 189

McLaren, I., Richardson, K.M., Wolfendale, A.W., 1988 ApJ 333, 821

McKee C.F., Zweibel E.G., 1992 ApJ 399, 551

Meinert D., 1992 Ph.D. Thesis Univ. Bonn (FRG)

Ohta K., Tomita A., Saito M., Sasaki M., 1993 PASJ 45, L21

Pagel B.E.J., Edmunds M.G., Smith G., 1980 MNRAS 193, 219

Pagel B.E.J., Simonson E.A., Terlevich R.J., Edmunds M.G., 1992 MNRAS 255, 325

Rayo J.F., Peimbert M., Torres-Peimbert S., 1982 ApJ 255, 1

Rice W., Boulanger F., Viallefond F., Soifer B.T., Freedman W.L., 1990 ApJ 358, 418

Roberts M.S., Haynes M.P., 1994 ARAA 32, 115

Rohlfs K. Kreitschmann J., Siegman B.C., Feitzinger J.V., 1984 A&A 137, 343

Rubio M., Garay G., Montani J., Thaddeus P., 1991 ApJ 368, 173

Rubio M., Lequeux J., Boulanger F., 1993 A&A 271, 9

Sage L.J., Salzer J.J., Loose H.-L., Henkel C., 1992 A&A 265, 19

Sakamoto S., 1996 ApJ 462, 215

Sasaki M., Ohta K., Saito M., 1990 PASJ 42, 361

Schwering P.B.W., 1988 Ph.D. Thesis, University of Leiden (NL)

Shaver P.A., McGee R.X., Newton L.M., Danks A.C., Pottasch S.R., 1983 MNRAS 204, 53

Skillman E.D., Kennicutt R.C., Hodge P.W., 1989a ApJ 347, 875

Skillman E.D., Terlevich R., Melnick J., 1989b MNRAS 240, 563

Stasinska G., Comte G., Vigroux L., 1986 A&A 154, 352

Strömgren B., 1939 ApJ 89, 526

Talent D.L., 1980 Ph.D. Thesis Rice University

Tacconi L.J., Young J.S., 1985 ApJ 290, 602

Thronson H.A., Hunter D.A., Telesco C.M., Harper D.A., Decher R., 1987 ApJ 317, 180

Thronson H.A., Hunter D.A., Telesco C.M., Greenhouse M., Harper D.A., 1988 ApJ 334, 605

Tosi M., Diaz A.I., 1990 MNRAS 246, 616

Ungerechts H., Thaddeus P., 1987 ApJS 63, 645

van der Hulst J.M., Sancisi R., 1988 AJ 95, 1354
van Driel W., de Graauw Th., de Jong T., Wesselius P.R., 1993 A&AS 101, 207
Verter F., Hodge P.W., 1995 ApJ 446, 616
Viallefond F., Boulanger F., Cox P., et al., 1992 A&A 265, 437
Vila-Costas M.B., Edmunds M.G., 1992 MNRAS 259, 121
Vilchez J.M., Pagel B.E.J., Diaz A.I., Terlevich E., Edmunds M.G., 1988 MNRAS 235, 633

Webster B.L., Smith, M.G., 1983 MNRAS 204, 473
Wilson C.D., 1994 ApJL 434, L11
Wilson C.D., Scoville N.Z., 1992 ApJ 385, 512
Young J.S., Gallagher J.S., Hunter D.A., 1984 ApJ 276, 476